DOSE3D: EGS4 Monte Carlo Code-Based Software for Internal Radionuclide Dosimetry

Isabelle Clairand, Marcel Ricard, Jean Gouriou, Mireille Di Paola and Bernard Aubert

Physics Department and Institut National de la Santé et de la Recherche Médicale (INSERM) Unité 494, Institut Gustave-Roussy, Villejuif; and Commissariat à l'Énergie Atomique (CEA), Gif sur Yvette, France

MIRDOSE3 software is currently the main tool available in clinical practice to evaluate absorbed dose in nuclear medicine. Because MIRDOSE3 provides dosimetric parameters for specific anatomic models that cannot be modified by the user, it cannot be used to obtain information concerning metastases or to consider patients whose anatomy differs significantly from that of the standard models. **Methods:** To address some of these inconveniences, we developed an original program based on the EGS4 Monte Carlo code, DOSE3D, which calculates dosimetric parameters for anthropomorphic phantoms defined with combinatorial geometry. DOSE3D allows the user to add spheres within the phantom for simulating tumors, to change the shape of one or more organs and, for organs defined by pair, to calculate individual dosimetric parameters for each organ. The program was validated for ^{131}I and ^{99m}Tc by calculating S values for the Medical Internal Radiation Dose (MIRD) adult male phantom and comparing these results with data provided by MIRDOSE3. Moreover, two studies were performed to illustrate DOSE3D features. The first one concerned the evaluation of the individual influence of two bone metastases (located in the pelvis and in the lower spine and containing ^{131}I) on testes in terms of S values compared with the influence on testes of other source organs (kidneys, liver, lungs, spleen, thyroid gland and urinary bladder contents). The second study determined the differences of S values between right and left lungs and right and left kidneys when ^{131}I is contained in the liver. **Results:** The DOSE3D S values were on average within 20% of the MIRDOSE3 results for both radionuclides. Regarding the bone metastases study, S(testes←metastases) and S(testes←any source organs) were of the same order of magnitude. In the second study, the S values ratio between right and left organs was 7.7 for the lungs and 5.2 for the kidneys. **Conclusion:** The agreement between DOSE3D and MIRDOSE3 results for most organs shows the validity of DOSE3D. The presented examples of calculation show that DOSE3D could provide additional data to dosimetric parameters given by MIRDOSE3 for a more patient-specific dosimetric approach.

Key Words: internal dosimetry; Monte Carlo simulation; combinatorial geometry; metastases; radiation protection

J Nucl Med 1999; 40:1517–1523

Accurate dosimetry is essential to ensure radiation protection of patients during nuclear medicine diagnostic procedures. Accurate dosimetry is also needed in treatment using radionuclide therapy for a better determination of the dose-response relationship and for avoiding critical organ toxicity (*1–3*). Because anatomy and biokinetics vary among subjects, individual morphological characteristics should be considered when calculating absorbed doses.

To determine the average absorbed dose at organ level, the formalism developed by the Medical Internal Radiation Dose (MIRD) Committee is widely considered as the reference method (*4*). This calculation method has been implemented in the MIRDOSE3 software (*5*) developed by Oak Ridge Associated Universities. Using tabulated specific absorbed fractions (SAFs) and radionuclide decay data, the main function of this software program is to provide estimates of the mean radiation dose per unit administered activity, given the source organ residence times, the radionuclide and using the specific anthropomorphic models described by Cristy and Eckerman (*6*) and by Stabin et al. (*7*). This software also provides the absorbed dose to isolated small unit density spheres, which are of interest in the dose calculation to a spherical tumor. Because MIRDOSE3 uses tabulated data, and the location of tumors cannot be known in advance, these spheres are not introduced in the anthropomorphic phantoms. Consequently, the dose to adjacent organs as a result of tumor activity and the dose to the tumor as a result of activity in adjacent tissues cannot be estimated using MIRDOSE3. Another software program, MABDOSE (*8–10*), addresses this problem by calculating S values for metastases as source or target organs, treating the tumor as a sphere within the Reference Man geometry and performing a Monte Carlo simulation in real time.

Others approaches, mostly dedicated to radioimmunotherapy, provide patient-specific dosimetry. The most sophisticated methods use functional information obtained from a three-dimensional set of images representing radionuclide distribution (SPECT/PET) combined with three-dimensional patient anatomy information obtained from CT or MRI (*11–15*).

The aim of this study was to design a system in the field of radiation protection dedicated to the improvement of patient dosimetry, in terms of S values, that would give information currently not provided by MIRDOSE3. Indeed,

Received Aug. 14, 1998; revision accepted Mar. 5, 1999.

For correspondence contact: Isabelle Clairand, PhD, Physics Department, Institut Gustave-Roussy, 39 rue Camille Desmoulins, 94805 Villejuif Cedex, France. For reprints contact: Marcel Ricard, PhD, Physics Department, Institut Gustave-Roussy, 39 rue Camille Desmoulins, 94805 Villejuif Cedex, France.

because MIRDOSE3 uses precalculated data, it provides dosimetric parameters for specific geometries that cannot be modified by the user. It is therefore not possible to obtain information concerning metastases or to consider patients whose anatomy differs significantly from that of the standard models. To address some of these inconveniences, we developed the DOSE3D program based on the EGS4 Monte Carlo code (*16*). For any radionuclide, this program calculates SAFs for any pair of source and target organs located in mathematical anthropomorphic phantoms defined using combinatorial geometry. DOSE3D also allows the user to add metastases within the phantom using spheres and to choose locations and sizes for these spheres. Moreover, using DOSE3D, it is possible to change the shape of one or more organ(s) to account for patient morphology and, with organs defined by pair, to calculate individual dosimetric parameters for each organ separately.

In this article, the DOSE3D program and the design of the MIRD adult male mathematical phantom using combinatorial geometry are described. The program then is validated by comparing the results it provides when using ^{131}I and ^{99m}Tc with those obtained using MIRDOSE3 for several source organs. Finally, two examples are used to illustrate the DOSE3D features.

MATERIALS AND METHODS

Program Description

The DOSE3D program, based on the EGS4 Monte Carlo code (*16*), was written to calculate SAFs at organ level for mathematical anthropomorphic phantoms. The S values are then deduced from the SAFs. The phantoms are described using the MORSE-CG combinatorial geometry (*17,18*). MORSE-CG subroutines were introduced in the DOSE3D program using the method proposed in the usercode UCSAMPCG (*16*) included in the EGS4 package. Activity in the source organ is assumed to be uniformly distributed. The site of the initial point of emission is randomly selected in the three directions in space in a parallelepiped including the source organ volume. The particles are followed until they escape the limits of the phantom or when their kinetic energy falls below an energy cutoff. The total energy deposited in each organ is scored so that the SAFs can be calculated.

Anthropomorphic Phantom Characteristics

We modeled the adult male phantom described by Cristy and Eckerman (*6*) using MORSE-CG combinatorial geometry. Combinatorial geometry is used to describe three-dimensional configurations with unions, differences and intersections of simple bodies. The skeleton and organs of the adult male phantom are presented in Figure 1. The phantom consisted of three different media: soft tissue (1.04 g/cm^3), lung (0.296 g/cm^3) and bone (1.4 g/cm^3). The chemical composition of each medium was similar to that described by Cristy and Eckerman (*6*).

The adult male phantom was slightly modified. Given the limited number of shapes available in the combinatorial geometry system, new models had to be found for the thyroid gland and the lower large intestine. We also introduced two organs, the prostate gland, using the model described by Stabin (*19*), and the eyes, which were modeled from the work of Bouchet et al. (*20*).

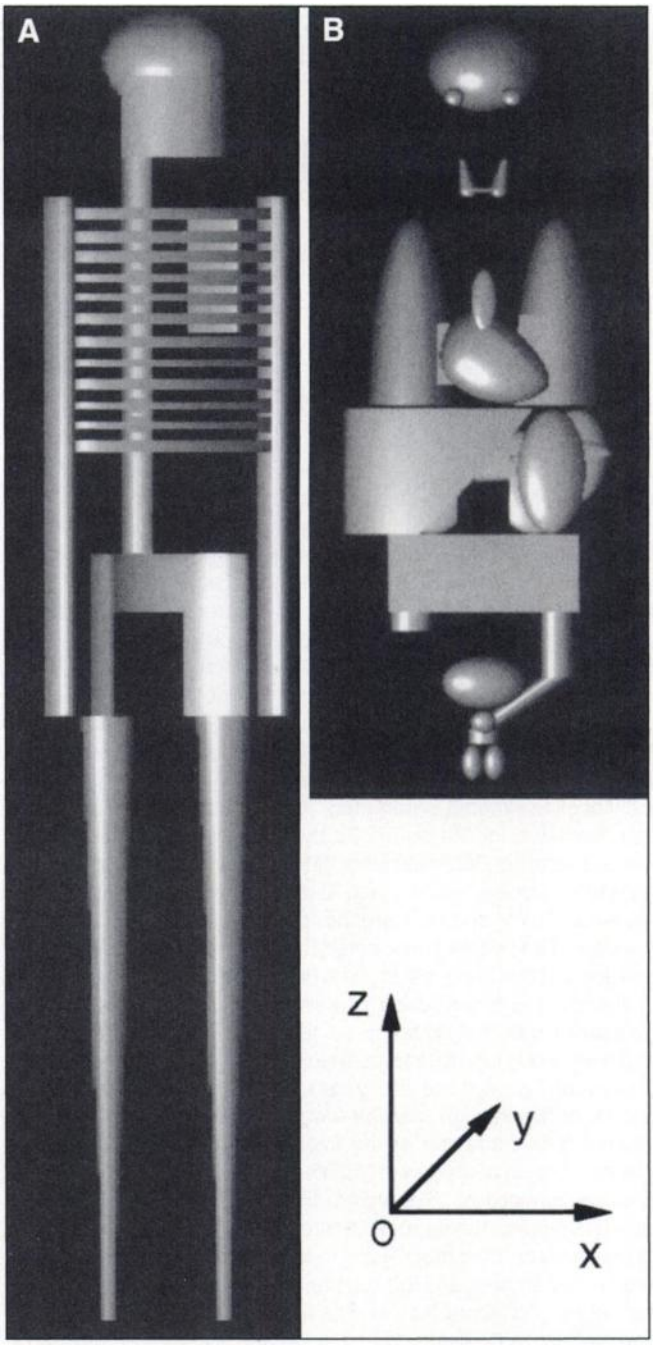

FIGURE 1. Representation of adult male phantom. (A) Skeleton. (B) Internal organs.

The phantom is described in a right-hand coordinate system with the origin at the center of the base of the trunk. In the following equations all dimensions are in centimeters.

The thyroid gland (original mass 20.7 g) was defined as the union of two elements, each composed of a half sphere topped by a truncated cone. These two elements were linked by a cylinder (Fig. 2).

The half sphere was defined by:

$$\begin{cases} \left[\frac{x \pm 1.80}{1.10}\right]^2 + \left[\frac{y + 4.00}{1.10}\right]^2 + \left[\frac{z - 71.10}{1.10}\right]^2 \le 1, \\ 70.00 \le z \le 71.10 \end{cases} \quad \text{Eq. 1}$$

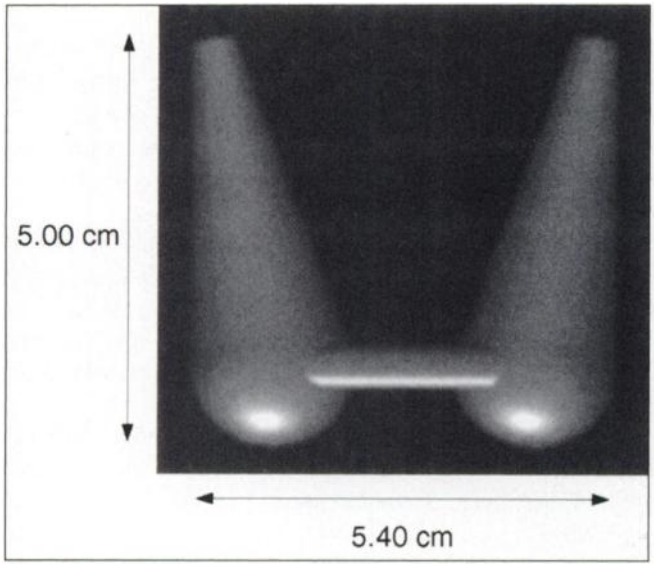

FIGURE 2. Thyroid gland model.

where the ± sign indicates positive for the right part and negative for the left part.

The truncated cone was defined as:

$$\begin{cases} \left[x \pm \left(1.80 + z\left(\frac{1.10 - 0.4}{3.9}\right)\right)\right]^2 \\ \quad + (y + 4.00)^2 \le \left[1.10 - z\left(\frac{1.10 - 0.4}{3.9}\right)\right]^2. \\ 71.10 \le z \le 75.00 \end{cases} \quad \text{Eq. 2}$$

The cylinder was defined by:

$$\begin{cases} \left[\frac{y + 4.80}{0.3}\right]^2 + \left[\frac{z - 71.10}{0.3}\right]^2 \le 1. \\ -1.80 \le x \le 1.80 \end{cases} \quad \text{Eq. 3}$$

The sigmoid part of the lower large intestine was represented as two elliptical cylinders (Fig. 3), whereas the descending colon remained unchanged.

The first part of the sigmoid colon was defined as a tilted elliptical cylinder. The wall of the first part of the sigmoid colon

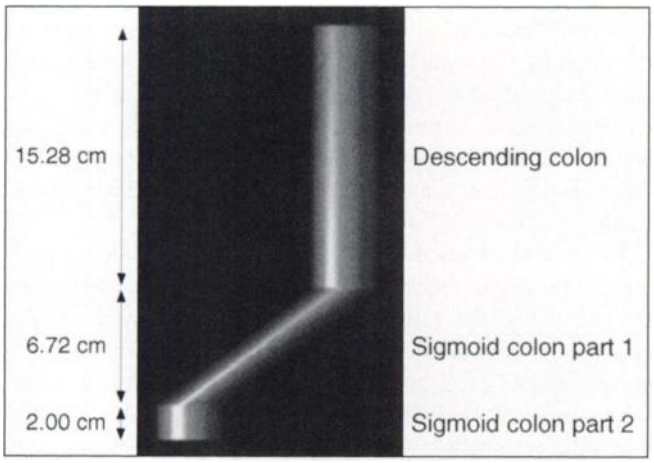

FIGURE 3. Lower large intestine model. Sigmoid colon is modeled using two elliptical cylinders (part 1 and part 2).

was specified using:

$$\begin{cases} \left[\frac{x - z\left(\frac{8.62}{6.72}\right)}{1.88}\right]^2 + \left[\frac{y - z\left(\frac{-2.36}{6.72}\right)}{2.13}\right]^2 \le 1 \\ \left[\frac{x - z\left(\frac{8.62}{6.72}\right)}{1.88 - 0.66}\right]^2 + \left[\frac{y - z\left(\frac{-2.36}{6.72}\right)}{2.13 - 0.66}\right]^2 \ge 1. \\ 2 \le z \le 8.72 \end{cases} \quad \text{Eq. 4}$$

The contents of the first part of the sigmoid colon were defined as the space within the inner elliptical cylinder:

$$\begin{cases} \left[\frac{x - z\left(\frac{8.62}{6.72}\right)}{1.88 - 0.66}\right]^2 + \left[\frac{y - z\left(\frac{-2.36}{6.72}\right)}{2.13 - 0.66}\right]^2 < 1. \\ 2 \le z \le 8.72 \end{cases} \quad \text{Eq. 5}$$

The second part of the sigmoid colon was described as a right angle elliptical cylinder, the wall of which was defined using:

$$\begin{cases} \left[\frac{x}{1.88}\right]^2 + \left[\frac{y}{2.13}\right]^2 \le 1 \\ \left[\frac{x}{1.88 - 0.66}\right]^2 + \left[\frac{y}{2.13 - 0.66}\right]^2 \ge 1. \\ 0 \le z \le 2 \end{cases} \quad \text{Eq. 6}$$

The contents of the second part of the sigmoid colon were defined as follows:

$$\begin{cases} \left[\frac{x}{1.88 - 0.66}\right]^2 + \left[\frac{y}{2.13 - 0.66}\right]^2 < 1. \\ 0 \le z \le 2 \end{cases} \quad \text{Eq. 7}$$

The wall and the contents volumes of this lower large intestine were 180 and 175 cm^3, respectively, corresponding to 187- and 182-g masses.

Two organs were added: the prostate gland and the eyes. The prostate gland was defined using Stabin's model (*19*) as a 1.54-cm radius sphere described by:

$$\left[\frac{x}{1.54}\right]^2 + \left[\frac{y + 4.50}{1.54}\right]^2 + \left[\frac{z - 2.93}{1.54}\right]^2 \le 1. \quad \text{Eq. 8}$$

The volume of the prostate gland was 15.3 cm^3 and its mass was 16 g.

The eyes were modeled from the work of Bouchet et al. (*20*), using spheres defined by:

$$\left[\frac{x \pm 3.40}{1.22}\right]^2 + \left[\frac{y + 7.50}{1.22}\right]^2 + \left[\frac{z - 83.00}{1.22}\right]^2 \le 1. \quad \text{Eq. 9}$$

The volume of each eye was 7.6 cm^3 and the corresponding mass was 7.9 g.

Program Validation

To evaluate this calculation method, some of our results were compared with those tabulated by MIRDOSE3. S values were

calculated for ^{131}I and ^{99m}Tc for the adult male model previously described. The source organs were the kidneys, liver, lungs, spleen, thyroid gland and urinary bladder (UB) contents. The target organs included all organs defined in the phantom and the remaining soft tissues.

The decay data of ^{131}I and ^{99m}Tc were taken from *MIRD: Radionuclide Data and Decay Schemes* (*21*). Photon and β particle transports were simulated by Monte Carlo methods, regardless of the position and dimensions of the source and the target organs. We sampled the cumulative probability density function of each β spectrum previously obtained from software (*22*) developed in the National Primary Standard Laboratory (Laboratoire Primaire des Rayonnements Ionisants, Gif sur Yvette, France).

Two situations were considered for electrons. For the kidneys, liver, lungs, spleen and thyroid gland as source organs, electron transport was not simulated by Monte Carlo calculations because the source organ dimensions greatly exceeded the electron range. The absorbed fraction was set to 1 when the source and target organ were the same and set to 0 otherwise. When the contents of the UB were the source and the UB wall was one of the targets, this approximation was not correct because part of the energy emitted by the contents obviously would be absorbed by the wall. In this case, electron transport was simulated. In addition, as for the other target organs, all energy absorbed by the wall was divided by the mass of the wall to obtain SAFs.

One million histories were simulated for each radiation component, i.e., photons, electrons and β particles. Particles were followed until they escaped the limits of the phantom or when their kinetic energy fell below 10 keV. The calculations were run on a PC Pentium Pro 200 MHz (Intel Corp., Santa Clara, CA). For one source organ, the simulation time was on average 6 h for ^{99m}Tc and 4 d for ^{131}I. The Monte Carlo calculations were performed in 10 batches of 100,000 histories, and the coefficient of variation (CV) was expressed as a percentage of the mean of the 10 absorbed fractions measured in each organ. Each batch was initialized with a different random generator seed.

Illustration of DOSE3D Features

Two examples of calculation were performed to illustrate the DOSE3D features. In the first study, we simulated two bone metastases located in the pelvis (META1) and in the lower spine (META2) by incorporating two 2-cm-diameter spheres within the adult male phantom. Monte Carlo simulations were performed in the case of ^{131}I uniformly distributed in each sphere using the same calculation parameters as those used for the program validation. Considering testes as the target organ, S(testes←META1) and S(testes←META2) were compared with S(testes←X), where X represented any other source organ taken individually (kidneys, liver, lungs, spleen, thyroid gland or UB contents).

The second calculation illustrated, for organs defined by pair, the ability of DOSE3D to calculate individual dosimetric parameters for each organ. Monte Carlo simulations were performed in the case of ^{131}I uniformly distributed in the liver. S values were determined and analyzed for the right and left lungs (462 and 536 g, respectively) and for the right and left kidneys (149.8 g each).

RESULTS

S values (mGy/MBq × s) and corresponding CV obtained using the DOSE3D and the MIRDOSE3 programs and the ratios MIRDOSE3 to DOSE3D are presented in Tables 1 and 2 for ^{131}I and ^{99m}Tc, respectively. Target organs are classified by weight. In MIRDOSE3, tabulated SAFs for electrons and β particles are estimated by the method used in *MIRD Pamphlet No. 11* (*23*), and tabulated SAFs for photons are the data published by Cristy and Eckerman (*6*). We referred therefore to the calculation methods in these two references to analyze the differences observed between our results and those given by MIRDOSE3.

Results on metastases are presented in Figure 4, where source organs are classified according to their distance from the testes. S(testes←META1) was 2.8E-07 mGy/MBq × s, and S(testes←META2) was 7.4E-09 mGy/MBq × s. Numerical values corresponding to S(testes←X) are presented in Table 1.

Results on the dosimetric study for organs defined by pair are presented in Figure 5. When ^{131}I was uniformly distributed in the liver, S values were 1.0E-06 and 1.3E-07 mGy/MBq × s for the right and left lungs, respectively. This means that the ratio between the radiation dose absorbed by the two lungs was 7.7. The S values were 1.3E-06 and 2.5E-07 mGy/MBq × s for the right and the left kidneys, respectively, corresponding to a ratio of 5.2.

DISCUSSION

Comparison with MIRDOSE3 S Values

DOSE3D and MIRDOSE3 estimates of organ self-doses were very similar, with ratios between 0.99 and 1.04 for all source organs and radionuclides. However, large discrepancies were observed in the UB wall when the UB contents were the source organ. The S value calculated by DOSE3D was four times lower for ^{131}I and two times lower for ^{99m}Tc than the S values from MIRDOSE3 because, in MIRDOSE3, SAFs for electrons and β particles are not calculated by Monte Carlo methods for hollow organs. Instead, the absorbed dose to the wall caused by activity in the contents is calculated as 50% of the average absorbed dose to the contents, as detailed in *MIRD Pamphlet No. 11* (*23*). This corresponds to the absorbed dose to the wall-contents interface. This conservative approach may overestimate absorbed doses for walled organs, as recently shown by Stubbs et al. (*24*). However, according to their results, our method of calculation, which involves dividing the energy absorbed by the wall by the entire mass of the wall, probably underestimates the dose to the radiosensitive cells located at some depth into the wall (*24*). Otherwise, the presence of β particles in the decay scheme of ^{131}I explains why discrepancies were greater for ^{131}I than for ^{99m}Tc, which is not a β emitter.

When considering the lower large intestine wall as a target organ, the discrepancies (ratio equal to 0.75 on average) obviously are the result of the new model used in our phantom. Our results were systematically higher that those of MIRDOSE3, except when the thyroid gland was the source organ for ^{131}I. In this case, the S value calculated by DOSE3D was 1.34 times lower. However, because the thyroid gland is far from the lower large intestine (>60 cm), the S value is too small to consider the ratio to be significant.

TABLE 1
S Values (mGy/MBq × s) Calculated by DOSE3D and Tabulated in MIRDOSE3 for ^{131}I

Target organs	Source organs: Kidneys				Liver				Lungs				Spleen				Thyroid gland				UB contents			
	DOSE3D	CV	MIRDOSE3	Ratio	DOSE3D	CV	MIRDOSE3	Ratio	DOSE3D	CV	MIRDOSE3	Ratio	DOSE3D	CV	MIRDOSE3	Ratio	DOSE3D	CV	MIRDOSE3	Ratio	DOSE3D	CV	MIRDOSE3	Ratio
Liver	8.09E-07	0.3	8.13E-07	1.01	2.06E-05	0.1	2.12E-05	1.03	4.82E-07	0.4	5.44E-07	1.13	1.90E-07	0.5	2.14E-07	1.13	3.50E-08	1.4	3.49E-08	1.00	4.52E-08	1.2	4.79E-08	1.06
Brain	1.91E-09	6.4	1.47E-09	0.77*	5.14E-09	2.9	5.50E-09	1.07*	2.96E-08	1.8	3.33E-08	1.13	5.13E-09	6.4	5.71E-09	1.11*	4.00E-07	0.4	4.18E-07	1.05	7.73E-11	19.3	1.33E-10	1.72*
Small intestine	6.04E-07	0.4	5.89E-07	0.98	3.31E-07	0.7	3.26E-07	0.98	5.34E-08	1.5	5.02E-08	0.94	2.90E-07	1.0	2.91E-07	1.00	4.08E-09	4.6	3.03E-09	0.74*	5.40E-07	0.5	5.73E-07	1.06
Lungs	2.00E-07	0.6	1.95E-07	0.98	5.36E-07	0.3	5.45E-07	1.02	3.23E-05	0.1	3.35E-05	1.04	4.49E-07	0.7	4.51E-07	1.00	2.77E-07	0.8	2.52E-07	0.91	7.61E-09	3.4	6.16E-09	0.81*
Heart wall	2.24E-07	0.9	2.27E-07	1.01	5.35E-07	0.6	6.32E-07	1.18	7.94E-07	0.5	1.18E-06	1.49	4.07E-07	0.7	4.36E-07	1.07	1.97E-07	1.2	1.35E-07	0.69	9.07E-09	4.3	1.03E-08	1.14*
Kidneys	1.12E-04	0.1	1.17E-04	1.04	7.80E-07	0.8	8.13E-07	1.04	2.10E-07	1.2	1.95E-07	0.93	1.83E-06	0.4	1.85E-06	1.01	1.50E-08	3.6	1.92E-08	1.28*	7.11E-08	2.0	8.00E-08	1.13
ULI wall	5.76E-07	1.1	5.78E-07	1.00	5.26E-07	0.4	5.13E-07	0.98	6.29E-08	3.2	6.36E-08	1.01	2.90E-07	2.0	2.82E-07	0.97	5.11E-09	8.5	5.94E-09	1.16*	4.34E-07	1.2	4.33E-07	1.00
LLI wall	1.99E-07	1.3	1.66E-07	0.83	8.29E-08	3.1	5.18E-08	0.62	2.13E-08	6.9	1.64E-08	0.77*	1.49E-07	1.7	1.34E-07	0.90	1.60E-09	20.3	1.99E-09	1.25*	3.17E-06	0.4	1.53E-06	0.48
Spleen	1.54E-06	0.6	1.85E-06	1.20	1.43E-07	2.0	2.14E-07	1.49	3.30E-07	1.8	4.51E-07	1.37	1.89E-04	0.1	1.93E-04	1.02	3.05E-08	3.7	3.10E-08	1.02	3.62E-08	3.8	4.28E-08	1.18
Stomach wall	6.11E-07	0.9	6.93E-07	1.13	3.06E-07	0.8	4.21E-07	1.37	2.65E-07	1.2	3.24E-07	1.22	1.96E-06	0.5	2.02E-06	1.03	1.68E-08	5.5	2.16E-08	1.29	7.24E-08	3.1	7.29E-08	1.01
Pancreas	9.79E-07	0.9	1.40E-06	1.43	5.87E-07	1.2	1.02E-06	1.74	4.08E-07	1.6	4.72E-07	1.16	3.32E-06	0.7	3.58E-06	1.08	2.78E-08	4.3	3.20E-08	1.15	4.97E-08	5.9	5.42E-08	1.09
UB wall	7.88E-08	5.0	7.43E-08	0.94	4.76E-08	5.5	5.00E-08	1.05	9.67E-09	12.2	8.75E-09	0.90*	3.80E-08	6.3	4.02E-08	1.06	2.36E-10	36.4	1.19E-09	5.05*	2.14E-05	0.4	8.72E-05	4.07
Testes	1.35E-08	8.1	1.90E-08	1.41	8.05E-09	16.9	1.02E-08	1.27*	1.66E-09	29.1	3.15E-09	1.89*	6.81E-09	12.3	1.30E-08	1.91*	3.01E-10	88.4	4.13E-10	1.37*	1.05E-06	1.7	1.02E-06	0.97
Thymus	3.20E-08	10.3	6.79E-08	2.12	1.60E-07	6.5	1.76E-07	1.10	3.68E-07	2.1	7.89E-07	2.14	5.53E-08	6.7	1.04E-07	1.88	3.06E-07	3.4	4.39E-07	1.44	2.12E-09	46.7	6.04E-09	2.85*
Thyroid gland	1.25E-08	14.7	1.92E-08	1.53*	3.00E-08	12.8	3.49E-08	1.17	3.07E-07	4.1	2.52E-07	0.82	3.22E-08	15.3	3.10E-08	0.96	1.52E-03	0.1	1.57E-03	1.03	4.48E-10	47.2	1.18E-09	2.63*

*Organs separated by distance ≥ 40 cm (R_{90}). R_{90} is defined as radius of sphere centered around point source in water within which 90% of source energy is absorbed.
CV = coefficient of variation (%); ULI = upper large intestine; LLI = lower large intestine; UB = urinary bladder.

TABLE 2
S Values (mGy/MBq × s) Calculated by DOSE3D and Tabulated in MIRDOSE3 for ^{99m}Tc

Target organs	Source organs: Kidneys				Liver				Lungs				Spleen				Thyroid gland				UB contents			
	DOSE3D	CV	MIRDOSE3	Ratio	DOSE3D	CV	MIRDOSE3	Ratio	DOSE3D	CV	MIRDOSE3	Ratio	DOSE3D	CV	MIRDOSE3	Ratio	DOSE3D	CV	MIRDOSE3	Ratio	DOSE3D	CV	MIRDOSE3	Ratio
Liver	2.52E-07	0.3	2.93E-07	1.16	3.17E-06	0.1	3.23E-06	1.02	1.93E-07	0.4	1.96E-07	1.01	5.45E-08	0.5	7.20E-08	1.32	8.80E-09	1.7	8.62E-09	0.98	1.16E-08	2.1	1.17E-08	1.01
Brain	2.20E-10	18.6	1.58E-10	0.72*	5.93E-10	8.2	8.14E-10	1.37*	6.04E-09	2.6	7.61E-09	1.26*	6.19E-10	10.3	5.18E-10	0.84*	1.26E-07	0.7	1.35E-07	1.07	3.00E-12	>95	5.93E-12	1.98*
Small intestine	2.17E-07	0.6	2.12E-07	0.98	1.18E-07	0.4	1.16E-07	0.98	1.44E-08	1.6	1.34E-08	0.93	1.02E-07	0.8	1.01E-07	0.99	6.09E-10	10.8	4.85E-10	0.80*	1.97E-07	0.5	2.24E-07	1.14
Lungs	5.91E-08	0.4	6.64E-08	1.12	1.99E-07	0.8	2.08E-07	1.05	3.65E-06	0.2	3.73E-06	1.02	1.59E-07	0.5	1.64E-07	1.03	9.29E-08	0.5	8.80E-08	0.95	1.23E-09	7.8	1.03E-09	0.83*
Heart wall	7.31E-08	1.1	8.20E-08	1.12	2.33E-07	0.9	2.32E-07	1.00	4.45E-07	0.6	4.38E-07	0.98	1.50E-07	1.2	1.67E-07	1.11	4.77E-08	1.8	4.32E-08	0.91	1.85E-09	7.9	2.22E-09	1.20*
Kidneys	1.37E-05	0.2	1.37E-05	1.00	2.76E-07	0.9	2.93E-07	1.06	6.07E-08	2.2	6.64E-08	1.09	5.91E-07	0.6	6.61E-07	1.12	2.99E-09	6.0	2.95E-09	0.99	1.90E-08	1.8	2.00E-08	1.05
ULI wall	2.15E-07	1.0	2.12E-07	0.99	1.91E-07	0.8	1.88E-07	0.98	1.66E-08	3.7	1.80E-08	1.08	1.02E-07	1.2	1.06E-07	1.04	5.43E-10	12.6	7.67E-10	1.41*	1.52E-07	1.0	1.60E-07	1.05
LLI wall	6.47E-08	2.7	5.48E-08	0.85	2.20E-08	4.0	1.44E-08	0.65	5.52E-09	4.7	3.29E-09	0.60*	4.78E-08	2.8	4.64E-08	0.97	2.98E-10	42.6	2.06E-10	0.69*	1.27E-06	0.5	5.77E-07	0.45
Spleen	5.32E-07	0.8	6.61E-07	1.24	5.14E-08	2.2	7.20E-08	1.40	1.07E-07	1.9	1.63E-07	1.53	2.32E-05	0.2	2.33E-05	1.00	7.22E-09	6.4	7.81E-09	1.08	9.61E-09	3.8	8.38E-09	0.87
Stomach wall	2.27E-07	0.8	2.52E-07	1.11	1.10E-07	1.5	1.48E-07	1.35	1.03E-07	1.8	1.19E-07	1.15	6.38E-07	0.7	7.73E-07	1.21	4.72E-09	9.6	3.70E-09	0.78*	1.73E-08	5.0	2.09E-08	1.21
Pancreas	3.38E-07	1.2	4.96E-07	1.47	2.20E-07	1.4	3.85E-07	1.75	9.73E-08	2.2	1.74E-07	1.79	1.21E-06	0.7	1.28E-06	1.06	7.61E-09	9.3	7.26E-09	0.95	1.32E-08	6.9	1.38E-08	1.05
UB wall	1.87E-08	7.9	1.87E-08	1.00	1.33E-08	5.0	1.16E-08	0.87	1.26E-09	22.7	1.33E-09	1.06*	9.75E-09	9.0	8.02E-09	0.82	5.00E-11	>95	9.62E-11	1.92*	5.28E-06	0.6	1.14E-05	2.16
Testes	2.47E-09	18.8	3.09E-09	1.25*	2.00E-09	24.8	1.57E-09	0.79*	2.37E-10	48.0	3.66E-10	1.54*	1.06E-09	25.0	2.17E-09	2.04*	1.50E-11	>95	2.31E-11	1.54*	3.53E-07	2.4	3.72E-07	1.06
Thymus	1.82E-08	10.7	1.73E-08	0.95	3.25E-08	9.5	5.92E-08	1.82	1.36E-07	3.9	2.84E-07	2.08	2.01E-08	12.2	3.88E-08	1.93	1.64E-07	5.4	1.62E-07	0.99	3.76E-10	71.6	8.04E-10	2.14*
Thyroid gland	2.13E-09	30.5	2.95E-09	1.39*	7.50E-09	21.9	8.62E-09	1.15*	9.86E-08	5.8	8.80E-08	0.89	6.16E-09	22.5	7.81E-09	1.27*	1.57E-04	0.4	1.57E-04	1.00	9.54E-11	88.4	9.54E-11	1.00*

*Organs separated by distance ≥ 35 cm (R_{90}). R_{90} is defined as radius of sphere centered around point source in water within which 90% of source energy is absorbed.
CV = coefficient of variation (%); ULI = upper large intestine; LLI = lower large intestine; UB = urinary bladder.

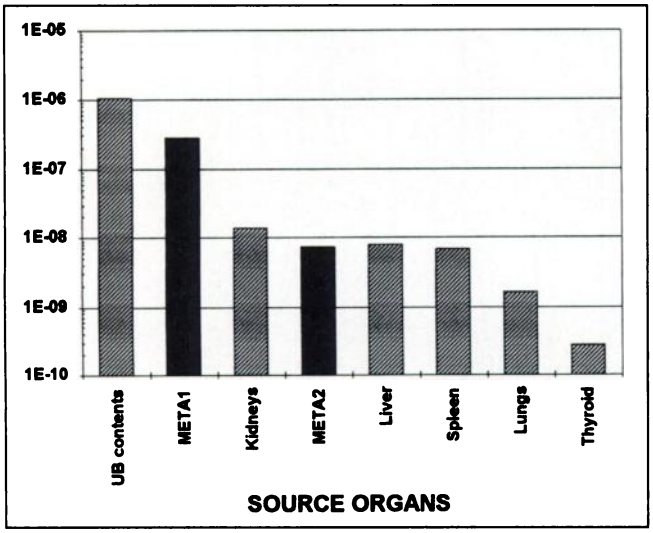

FIGURE 4. S(testes←META1) and S(testes←META2) compared with S(testes←other source organs) for ^{131}I. Metastases META1 and META2 are located in pelvis and in lower spine, respectively. The y-axis is S (mGy/MBq × s).

When the target organ is distant from the source organ, the energy absorbed by the target organ is low, and results obtained by a Monte Carlo method may not be reliable if the number of primary photons is too low. We considered the radius R_{90} of the sphere centered around a point source in water within which 90% of the source energy is absorbed as a threshold distance. According to *ICRU Report 32* (*25*), R_{90} equals 40 cm for ^{131}I and 35 cm for ^{99m}Tc.

For the source-target pairs in which centroids were more than R_{90} away (indicated with an asterisk in Tables 1 and 2), substantial disagreements between DOSE3D and MIRDOSE3 were observed. This is because, for these source-target pairs, the point-source kernel method associated with correction factors was used in MIRDOSE3, whereas DOSE3D used only Monte Carlo calculations. In the case of distant organs, S values determined with DOSE3D are assumed to be reliable, because CVs are less than 50% in most cases (usual reliability criterion [*23,26*]). However, for several source-target pairs separated by a long distance, CVs are greater than 50%. This is observed for the couple testes←thyroid gland for ^{131}I and for the couples UB wall←thyroid gland, testes←thyroid gland, brain←UB contents, thymus←UB contents and thyroid gland←UB contents for ^{99m}Tc. The fact that ^{99m}Tc emits photons of energy significantly lower than those emitted by ^{131}I explains why results are less reliable for ^{99m}Tc. Consequently, in these extreme situations, point-kernel techniques are obviously more accurate than Monte Carlo calculations.

For small target organs (spleen, pancreas, testes, thymus and thyroid gland), there were some discrepancies between our results and those from MIRDOSE3 regardless of source. This is because, for these organs, DOSE3D uses only direct Monte Carlo calculations, whereas MIRDOSE3 relies on data obtained using the reciprocal principle (*26*).

For all other source-target pairs, i.e., close organs with weight ≥ 300 g, S values calculated using DOSE3D and MIRDOSE3 agreed well, with an average difference of 8%.

Influence of Metastases on Dosimetric Parameters

The order of magnitude of metastatic S values is comparable with those of the other source organs. The S value for the pelvis metastasis is quite close to that of UB contents and is greater than other organ S values. The contribution of META2 is lower than those of the UB contents and kidneys because of its location but is equal to or higher than other organ S values. This example of calculation shows that the influence of metastases on dosimetric parameters may be significant. Consequently, metastases should be con-

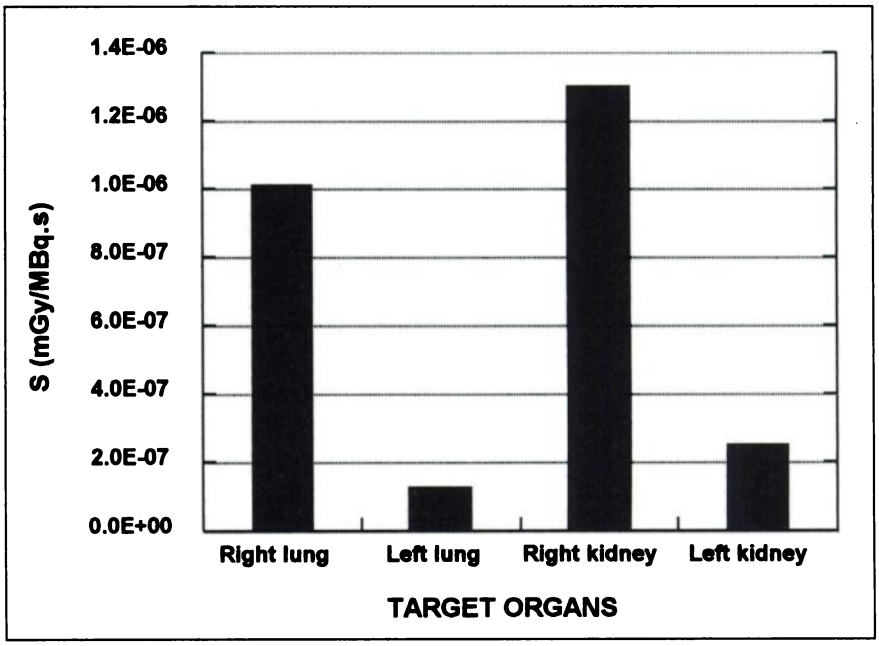

FIGURE 5. S values corresponding to right and left lungs and right and left kidneys when ^{131}I is uniformly distributed in liver.

sidered as source regions in absorbed dose calculations as other body organs are.

Organs Defined by Pair

In the case of the liver as source organ, the dose received by the right organs is considerably higher than that received by those on the left. Such differences indicate the importance of considering each organ in a pair individually, a technique made possible using DOSE3D. Because of this feature, DOSE3D is appropriate for calculation of dosimetric parameters for patients who have undergone the ablation of one of the two organs, a situation not unusual in patients with cancer.

CONCLUSION

We have developed an EGS4 Monte Carlo code-based program, DOSE3D, that calculates the specific absorbed fractions and S values for anthropomorphic phantoms defined using combinations of simple bodies.

DOSE3D results were compared with those provided by MIRDOSE3 for the adult male phantom with ^{131}I and ^{99m}Tc uniformly distributed in the kidneys, liver, lungs, spleen, thyroid gland and UB contents. The agreement between DOSE3D and MIRDOSE3 results for most organs showed the validity of our program and the accuracy of the geometric models based on combinations of simple bodies.

The main features of DOSE3D are the ability to add new regions within the phantoms, such as tumors, and to modify existing organs to calculate dose estimates that are more specific to each patient.

ACKNOWLEDGMENTS

The authors are grateful to Michael Stabin and Keith Eckerman for giving us information concerning the simulation parameters used to obtain the data in MIRDOSE3. The authors are indebted to Irène Buvat and Robert Di Paola for helpful discussions and to Lorna Saint-Ange and Ingrid Kuchenthal for editing the manuscript. This work was supported by a grant from the Institut de Formation Supérieure BioMédicale and by Electricité de France, contract no. 1H6293/D332.

REFERENCES

1. International Commission on Radiological Protection. Recommendations of the International Commission on Radiological Protection. ICPR Publication 60. *Ann ICRP.* 1990;21.
2. International Commission on Radiological Protection. *Radiological Protection and Safety in Medicine.* ICPR Publication 73. Oxford, England: Pergamon Press; 1996.
3. *International BASIC SAFETY STANDARDS for Protection Against Ionizing Radiation and for the Safety of Radiation Sources.* Safety Series no. 115. Vienna, Austria: International Atomic Energy Agency; 1996.
4. Loevinger R, Budinger TF, Watson EE. *MIRD Primer for Absorbed Dose Calculations.* Revised ed. New York, NY: Society of Nuclear Medicine; 1991.
5. Stabin MG. MIRDOSE: Personal computer software for internal dose assessment in nuclear medicine. *J Nucl Med.* 1996;37:538–546.
6. Cristy M, Eckerman KF. *Specific absorbed fractions of energy at various ages from internal photons sources.* ORNL Report ORNL/TM-8381 V1-V7. Oak Ridge, TN: Oak Ridge National Laboratory; 1987.
7. Stabin MG, Watson EE, Cristy M, et al. *Mathematical Models and Specific Absorbed Fractions of Photon Energy in the Nonpregnant Adult Female and at the End of Each Trimester of Pregnancy.* ORNL Report ORNL/TM-12907. Oak Ridge, TN: Oak Ridge National Laboratory; 1995.
8. Johnson TK. MABDOS: a generalized program for internal radionuclide dosimetry. *Comput Methods Programs Biomed.* 1988;27:159–167.
9. Johnson TK, Vessella RL. On the possiblity of "real-time" Monte Carlo calculations for the estimation of absorbed dose in radioimmunotherapy. *Comput Methods Programs Biomed.* 1989;29:205–210.
10. Johnson TK, Andl G, Berman B. MABDOSE: a program for the calculation of internal dose [abstract]. *J Nucl Med.* 1995;36(suppl):182P.
11. Sgouros G, Chiu S, Pentlow KS, et al. Three-dimensional dosimetry for radioimmunotherapy treatment planning. *J Nucl Med.* 1993;34:1595–1601.
12. Giap HB, Macey DJ, Podoloff DA. Development of a SPECT-based three-dimensional treatment planning system for radioimmunotherapy. *J Nucl Med.* 1995;36:1885–1894.
13. Kolbert KS, Sgouros G, Scott AM, et al. Implementation and evaluation of patient-specific three-dimensional internal dosimetry. *J Nucl Med.* 1997;38:301–308.
14. Tagesson M, Ljungberg M, Strand S-E. A Monte Carlo program converting activity distributions to absorbed dose distributions in a radionuclide treatment planning system. *Acta Oncol.* 1996;35:367–372.
15. Furhang EE, Chui CS, Kolbert KS, Larson SM, Sgouros G. Implementation of a Monte Carlo dosimetry method for patient-specific internal emitter therapy. *Med Phys.* 1997;24:1163–1172.
16. Nelson WR, Hirayama H, Rogers DWO. *The EGS4 Code System.* SLAC report no. 265. Palo Alto, CA: Stanford University Press; 1985.
17. Nelson WR, Jenkins TM. Geometry methods and packages. In: Jenkins TM, Nelson WR, Rindi A, eds. *Monte Carlo Transport of Electrons and Photons.* New York, NY: Plenum Press; 1988.
18. Straker EA, Stevens PN, Irving DC, Cain VR. *MORSE-CG: general purpose Monte Carlo multigroup neutron and gamma-ray transport code with combinatorial geometry.* Report CCC-203. Oak Ridge, TN: Radiation Shielding Information Center (ORNL); 1976.
19. Stabin MG. A model of the prostate gland for use in internal dosimetry. *J Nucl Med.* 1994;35:516–520.
20. Bouchet LG, Bolch WE, Weber DA, Atkins HL, Poston JW Sr. A revised dosimetric model of the adult head and brain. *J Nucl Med.* 1996;37:1226–1236.
21. Weber DA, Eckerman KF, Dillman LT, Ryman JC. *MIRD: Radionuclide Data and Decay Schemes.* New York, NY: Society of Nuclear Medicine; 1989.
22. Cassette P. Programme SPEBETA. *Note technique interne.* Report CEA/LPRI/92/307. Saclay, France: Commissariat à l'Energie Atomique; 1992.
23. Snyder WS, Ford MR, Warner GG, Watson SB. *'S,' Absorbed Dose per Unit Cumulated Activity for Selected Radionuclides and Organs.* MIRD pamphlet no. 11. New York, NY: Society of Nuclear Medicine; 1975.
24. Stubbs JB, Evans JF, Stabin MG. Radiation absorbed doses to the walls of hollow organs. *J Nucl Med.* 1998;39:1989–1995.
25. International Commission on Radiation Units and Measurements. *Methods of Assessment of Absorbed Dose in Clinical Use of Radionuclides.* ICRU Report 32. Washington, DC; International Commission on Radiological Units; 1979.
26. Cristy M. Applying the reciprocal dose principle to heterogeneous phantoms: practical experience from Monte Carlo studies. *Phys Med Biol.* 1983;28:1289–1303.